JOURNAL OF PETROLOGY | VOLUME 46 | NUMBER 8 | PAGES 1525–1541 | 2005 | doi:10.1093/petrology/egi024

Crystal Size Distributions (CSD) in Three Dimensions: Insights from the 3D Reconstruction of a Highly Porphyritic Rhyolite

A. MOCK* AND D. A. JERRAM

DEPARTMENT OF EARTH SCIENCES, UNIVERSITY OF DURHAM, SOUTH ROAD, DURHAM DH1 3LE, UK

RECEIVED JUNE 10, 2004; ACCEPTED FEBRUARY 8, 2005
ADVANCE ACCESS PUBLICATION MARCH 18, 2005

Growth histories and residence times of crystals in magmatic systems can be revealed by studying crystal sizes, size distributions and shapes. In this contribution, serial sectioning has been employed on a sample of porphyritic rhyolite from a Permo-Carboniferous laccolith from the Halle Volcanic Complex, Germany, to reconstruct the distribution of felsic phenocrysts in three dimensions in order to determine their true shapes, sizes and three-dimensional size distributions. A model of all three phenocryst phases (quartz, plagioclase, K-feldspar) with 217 crystals, and a larger model containing 1599 K-feldspar crystals was reconstructed in three dimensions. The first model revealed a non-touching framework of crystals in three dimensions, suggesting that individual crystals grew freely in the melt prior to quenching of the texture. However, crystal shapes are complex and show large variation on a Zingg diagram (intermediate over long axis plotted against short over intermediate axis). They often do not resemble the crystallographic shapes expected for phenocrysts growing unhindered from a melt, indicating complex growth histories. In contrast, the three-dimensional size distribution is a simple straight line with a negative slope. Stereologically corrected size distributions from individual sections compare well with stereologically corrected size distributions obtained previously from the same sample. However, crystal size distribution (CSD) data from individual sections scatter considerably. It is shown that CSDs can be robustly reproduced with a sampling size of greater than ~200 crystals. The kind of shape assumed in stereological correction of CSDs, however, has a large influence on the calculation and estimation of crystal residence times.

KEY WORDS: *3D reconstruction; crystal shapes; CSD; porphyritic rhyolite; quantitative petrography*

INTRODUCTION

Quantifying textures of igneous rocks

Igneous rocks are commonly crystalline, developing from the crystallization of magmas by a complex interplay of crystal nucleation and growth. In relatively quickly cooled volcanic rocks and shallow intrusions, the resultant textures of crystal phases may be rapidly frozen in. In other examples, igneous textures result from slow cooling and crystallizing conditions at depth. A major key to understanding the formation of igneous rocks is to link their textures to processes known or assumed to be active during their genesis. For this purpose, the arrangement of the constituents of the rocks (i.e. the spatial arrangement of mineral grains), the three-dimensional (3D) size distribution of crystals present and the nature of the constituents (geochemistry and mineralogy) must be quantified (for an overview, see, among others, Renzulli & Santi, 1997; Smith, 1998; Hammer *et al.*, 1999, 2000; Jerram & Cheadle, 2000; Kuscu & Floyd, 2001). In the following discussion, a number of abbreviations are used; these are defined in Table 1.

Topics such as mixing of magmas with different crystal populations (Higgins & Roberge, 2003), effusion rates and magma system volumes (Resmini & Marsh, 1995) and magma chamber processes (Tomiya & Takahashi, 1995) are but a few examples of the application of quantitative textural investigation to resolve questions about the origin of igneous rocks. However, thus far, quantification of inherently 3D igneous textures has been inhibited by general limitation to two-dimensional (2D) sections through a rock. Such sections are sufficient to

*Corresponding author. Telephone: +44-191–3342281. Fax: +44-191–3342301. E-mail: alexander.mock@durham.ac.uk. Previously: Institut für Geologie, Technische Universität Bergakademie Freiberg, Bernhard-von-Cotta-Str. 2, 09599 Freiberg, Germany.

Table 1: Parameters used in this study and their abbreviations in the text

2D	Two-dimensional
3D	Three-dimensional
CT	X-ray computed tomography
CSD	Crystal size distribution
CSD_{2D}	Size distribution from a 2D section of a sample
$CSD_{3D,cor}$	Stereologically corrected CSD_{2D}
CSD_{3D}	Size distribution determined from a 3D reconstruction
CL	Characteristic length of a crystal population from CSD slope
L	Crystal size
L_{max}	Maximum crystal size, determined from CSD
N	population density of crystals (number per volume per size)
R^2	Regression coefficient: $R = \frac{n(\sum XY)-(\sum X)(\sum Y)}{\sqrt{\left(n\sum X^2-(\sum X)^2\right)\left(n\sum Y^2-(\sum Y)^2\right)}}$ X, Y: data values; n: number of data points
RGB	Red, green and blue colour values in digital images
d_{sphere}	Diameter of a sphere
$c_{ellipsoid}$	Longest axis of an ellipsoid
KF	K-feldspar
PL	plagioclase
QZ	quartz
HVC	Halle Volcanic Complex
SHRIMP	Sensitive high-resolution ion microprobe

determine the bulk abundances of phases with precision (Delesse, 1848; Higgins, 2002), but especially in crystal size distribution (CSD) studies, correction for 2D–3D effects is necessary (Higgins, 2000). This has been limited in previous studies to a purely dimensional approach (raising the number of grains per size bin per unit area to the power of 1·5 to obtain number per size bin per unit volume, e.g. Marsh, 1988). Stereology—the mathematical dimensional conversion of size distributions—has brought major improvements to correction methods (e.g. Underwood, 1970; Elias & Hyde, 1983; Sahagian & Proussevitch, 1998; Higgins, 2000). However, the true 3D arrangement of complexly shaped natural particles in any opaque solid remains obscure. Methods do exist to make a rock's interior immediately available for observation in 3D. These include X-ray computed tomography (CT) (Denison & Carlson, 1997; Denison *et al.*, 1997; Ketcham & Carlson, 2001) and confocal microscopy (Petford *et al.*, 2001; Castro *et al.*, 2003) as non-destructive techniques, or serial sectioning or erosion as a destructive method (Bryon *et al.*, 1995; Cooper & Hunter, 1995; Marschallinger, 1998; Herbert & Jones, 2001). However, CT and confocal techniques are limited to rather small sample sizes. Tomography additionally requires a contrast in X-ray attenuation between the individual phases to be resolved in the rock and its matrix. Serial sectioning or erosion allows larger samples and larger grain sizes to be reconstructed, but also takes more time and is limited in resolution by the number of grinding steps.

In recent years, application of CSD analysis to igneous petrology has provided important new insights into magmatic processes (Cashman & Marsh, 1988; Marsh, 1988, 1998; Randolph & Larson, 1988). In this technique, the 3D size distribution of crystals in a rock ($CSD_{3D,cor}$) is calculated by measuring the 2D size distribution in cross-section (CSD_{2D}) and employing stereological techniques to convert 2D observations into 3D (Higgins, 2000). Such crystal size data can then be used to determine magma residence times, crystallization history and mixing events between different crystal populations, especially in combination with geochemical microanalysis (Higgins, 1996; Zellmer *et al.*, 1999; Cooper & Reid, 2003). A direct method for measuring CSD_{3D} in thick thin-sections has been proposed by Castro *et al.* (2003). This method is restricted to the measurement of microlites smaller than the thickness of thin sections ($\sim$30 μm), and to samples with low crystallinity. Nevertheless, Castro *et al.* (2003) have shown that CSDs determined from intersection distributions with stereological methods (Underwood, 1970; Peterson, 1996; Higgins, 2000) compare reasonably well with true 3D CSD, if the extreme large and small sizes of the given distributions are not incorporated into the analysis. Clearly, better examples of true 3D crystal populations are desirable to help refine the methods of 3D reconstruction and to test existing conversion techniques from 2D to 3D.

In this study, the phenocryst population in a single sample of a highly porphyritic subvolcanic rhyolite from the Permo-Carboniferous Halle Volcanic Complex (HVC, Fig. 1), is investigated. The true 3D texture of the phenocrysts is reconstructed digitally using a combination of serial grinding, imaging and 3D modelling software. The aim is to determine the shape, size and spatial distribution of felsic phenocrysts (QZ, PL, KF) in 3D, to compare these data with previously determined 2D textural data (Mock *et al.*, 2003), and to investigate methods of 3D textural analysis more thoroughly. The subsequent discussion focuses on the use of such 3D textural analysis techniques and the advantages and pitfalls of 2D versus 3D CSD measurements.

Geological overview of sample locality

The HVC is situated in the Saale Basin in Eastern Germany—one of several late Palaeozoic transtensional volcano-sedimentary basins in the area of the decaying Variscan orogen (Eigenfeld & Schwab, 1974; Lorenz & Nicholls, 1984). Magmatism here culminated 294–307 Myr ago with the emplacement of voluminous ($\sim$210 km^3), porphyritic rhyolitic laccoliths (Landsberg,

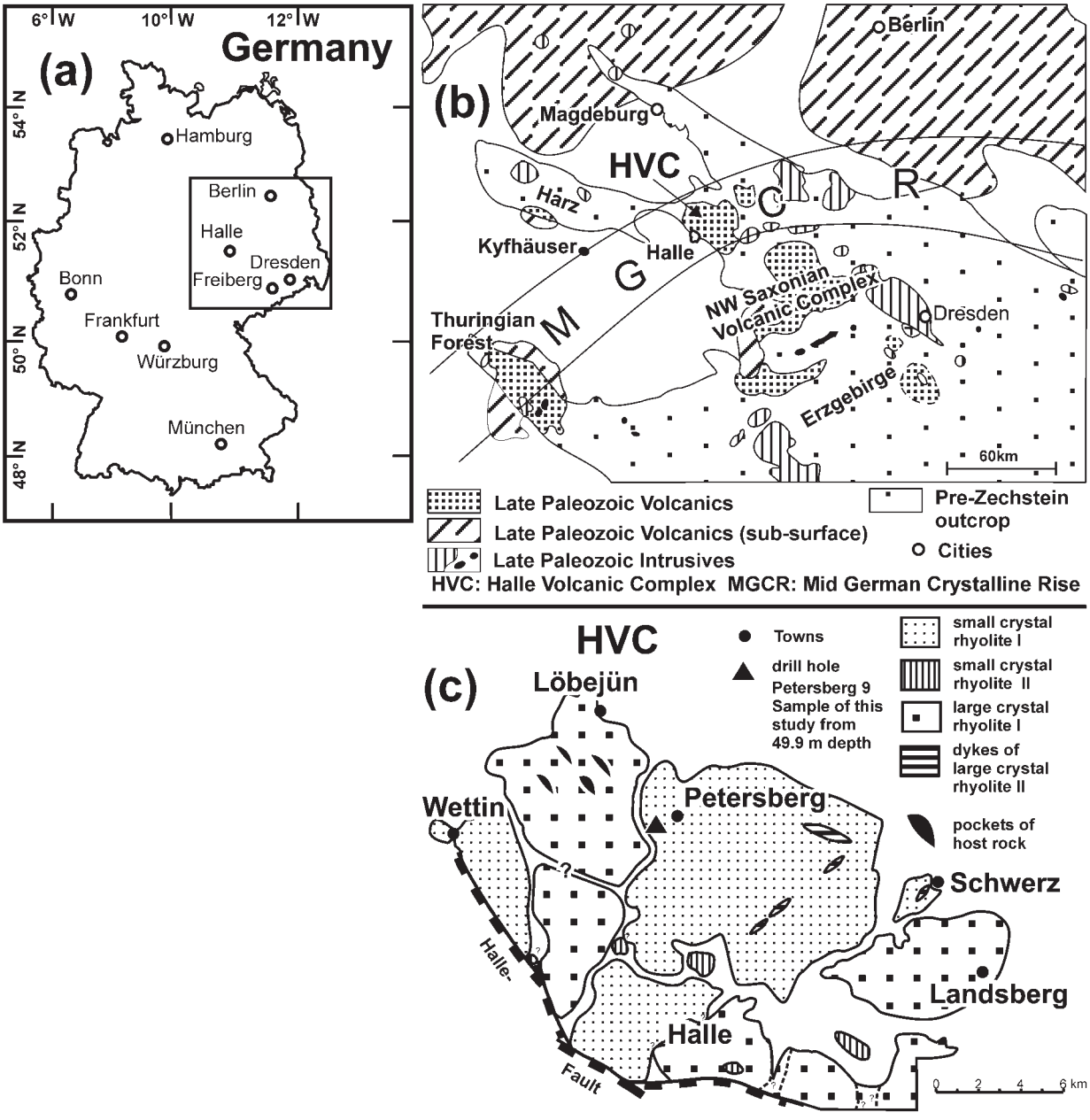

Fig. 1. Sample location and general geology of the study area around Halle, Germany.

Löbejün, Petersberg, Wettin, Schwerz units; Fig. 1, Breitkreuz & Kennedy, 1999; Breitkreuz & Mock, 2004). Of these laccolith units, the Löbejün and Landsberg units have up to ~30 mm long feldspar phenocrysts; the Landsberg unit also contains a variant with smaller phenocrysts compatible with the Wettin and Petersberg units (~5–10 mm). Within the Wettin unit, small schlieren-like domains with larger phenocrysts (~30 mm) can be found. The Schwerz unit is slightly older and textures are more varied than those of the other units (Fig. 1c). Felsic phenocryst contents vary from 10 to 25% by volume for small crystals and from 20 to 30% for large phenocryst varieties.

The Petersberg laccolith is the largest laccolith in the HVC with an estimated volume of ~60 km^3. It is approximately 400–500 m thick and around 10 km × 10 km in plan view (Fig. 1), and probably consists of several individual laccolithic intrusions (Breitkreuz & Mock, 2004). It formed 294 ± 3 Myr ago [U–Pb SHRIMP dating by Breitkreuz & Kennedy (1999)]. A detailed investigation of the spatial relationships and CSDs of phenocrysts in the Petersberg laccolith has

revealed an emplacement mechanism consisting of at least two magma batches without major cooling between them (Mock *et al.*, 2003). The modal abundance of phenocrysts is very uniform throughout the laccolith.

For the purpose of this study, a sample has been taken from a depth of 49·9 m close to the western lateral contact of the Petersberg laccolith (drill-core Petersberg 9/60; Fig. 1; sample 90499 of Mock *et al.*, 2003). At this location, the laccolith has a thickness of 300 m, measured from the present-day surface. However, contact textures in outcrops close to the drilling site (spherulites, perlitic groundmass) suggest a level of erosion within the upper third of the laccolith. Therefore, the sample probably represents the upper part, but not necessarily the immediate upper contact of the laccolith (Fig. 1). The entire Halle laccolith complex has been intensively studied using various methods of quantitative petrography (Mock *et al.*, 2003, 2005), thus providing an excellent database for comparison with the dataset presented here. Furthermore, the textures of the porphyritic rhyolite are readily examinable and analysable using only a binocular microscope and the procedures described below. The rhyolite is neither particularly fresh, nor does it display particularly simple textures, making it a general example for the kind of analysis presented here.

PROCEDURE OF 3D RECONSTRUCTION

A rectangular slab of ~7·5 cm × 8 cm × 4 cm was cut from the sample. One of the slab's surfaces was scanned with a conventional flat-bed scanner at 400 dpi, giving a pixel size of 0·0635 mm (0·004 mm^2). This set the lower limit for the size of a phenocryst cross-section recognizable in the scanned image. KF, PL and QZ phenocrysts were identified in the sample and the scanned image, and manually marked with false colours on the digital image using a drawing tablet (RGB values: KF: 255,0,0; PL: 255,255,0; QZ: 0,0,0). Images were analysed using KS300 (KONTRON ELEKTRONIK Imaging System) software for image analysis of manually classified images and Higgins' (2000) software CSDCorrection 1.36 for stereological correction yielding $CSD_{3D,cor}$ (see also Mock *et al.*, 2003). Additionally, image analysis provided modal abundances of phenocryst phases from the sum of the phenocrysts' areas divided by the total sample area.

The surface of the slab was then ground down for 45 min using an LP-40 lapping machine (Logitech Ltd, Glasgow), set to a pressure of 3·5 kg/sample and a speed of 70 rounds/min, and with SiC as grinding powder, with a grain size of 600 mesh and a water dispersion agent. Of the sample, 300–1000 μm were ground away at each step, as measured at the four corners of the sample slab with a vernier calliper (Table 2). After each of the 10 grinding steps, the slab was scanned as described above. In that way, 11 false colour images of the phenocrysts in the sample were retrieved (Fig. 2; Table 2).

False colour images were assigned grid coordinates for each pixel, using the software ENVI (Research Systems, Inc, Boulder, Colorado, USA); control points were the corners of the slab, defined as a single pixel on the false colour images. Coordinates for the sample image were chosen arbitrarily from a rectangular reference grid (e.g. Universal Transversal Mercator) and scaled to the sample size. Each cross-section of a phenocryst was converted into a polygon with a known location in the section area. One pixel (i.e. 0·004 mm^2 of the original sample) corresponded to 1 m^2 in the scaled model. This scaling was necessary in order to apply the rectangular reference grid (usually on a meter scale) and to incorporate the data into the 3D modelling software GOCAD (http://gocad.ensg.inpl-nancy.fr), which can read only a limited number of decimal places. Each sample section was given a coordinate value for the vertical dimension in GOCAD corresponding to the section spacing converted into model scale as mentioned above (see Table 2).

About 20% of the phenocrysts have been fractured and the fragments slightly rotated and partly annealed again during ascent and emplacement of the magma, possibly as a result of degassing early in its crystallization history (Fig. 3; Best & Christiansen, 1997; Mock *et al.*, 2005). However, the fragments were not separated from each other and it is possible to link these fragments in 3D reconstructions to form one closed surface representing the original crystal (see Figs 2 and 3 and the Electronic Appendix, available at http://www.petrology.oupjournals.org).

Sections representing the same phenocryst in different layers were identified and connected into a 3D closed surface using a digital smooth interpolation algorithm (DSI; compare Mallet, 1992) implemented in the GOCAD software (Figs 4 and 5). Polygons present in only one section (hereafter, singular sections) clearly represent phenocrysts smaller than the section spacing. These were doubled and set off in a negative and positive *z*-direction, with a value less than the section spacing at that position, in order to create a 3D closed surface. Thus, singular sections are all represented by prisms in the 3D model. This process is required in order to estimate a volume and size for the smaller crystals. CSD_{3D}, with and without the inclusion of crystals modelled from singular sections, are compared to show that they do not differ significantly (see below). Crystals touching the edge of the sample volume were not included into the CSD analysis. In this way, 3D models were generated of (1) a small volume, including 217 crystals of all three phases for testing their spatial relationships; and (2) 1599 KF phenocrysts, in order to extract 3D size distribution information (Fig. 5a–d). In the larger volume, 1282

Table 2: Properties of serial sections (scaled = z-coordinate in 3D model)

No.	Area (mm^2)	Spacing (mm)	Scaled (m)	CL (mm)	Intercept	L_{max} (mm)	Modal %	No. of grains
(*a*) *Textural parameters of KF*								
1	5879	0·4	0·0	0·80	0·46	8·45	4·8	1251
2	5860	0·4	6·3	0·94	0·18	8·45	7·8	816
3	5898	0·4	12·6	0·96	0·25	10·64	6·1	979
4	5854	0·6	22·1	0·86	0·28	8·45	6·5	892
5	5849	0·5	29·9	0·81	0·41	8·45	4·6	1118
6	5871	1·0	45·7	0·80	0·36	8·45	5·4	1001
7	5942	0·4	52·0	0·78	0·35	6·71	4·6	990
8	5898	0·3	56·7	0·78	0·36	6·71	5·2	990
9	5913	0·3	61·4	0·77	0·39	6·71	8·3	1047
10	5932	0·3	66·1	0·79	0·36	6·71	4·5	1046
11	6067	0·3	70·9	0·76	0·36	7·58	7·1	956

No.	CL (mm)	Intercept	L_{max} (mm)	Modal %	No. of grains
(*b*) *Textural parameters of PL for serial sections*					
1	0·75	0·61	8·45	3·3	1642
2	0·87	0·25	8·45	4·5	1107
3	0·81	0·39	8·45	4·0	1230
4	0·83	0·26	6·71	5·0	887
5	0·76	0·47	8·45	4·1	1171
6	0·86	0·33	8·45	4·4	1156
7	0·81	0·34	8·45	3·7	1168
8	0·79	0·36	8·45	3·6	1127
9	0·81	0·25	8·45	7·0	1045
10	0·79	0·37	8·45	3·9	1173
11	0·76	0·40	7·58	6·7	1130

No.	CL (mm)	Intercept	L_{max} (mm)	Modal %	No. of grains
(*c*) *Textural parameters of QZ for serial sections*					
1	0·57	0·41	4·74	4·7	716
2	0·74	0·13	4·74	5·4	411
3	0·70	0·16	4·74	5·5	498
4	0·75	0·11	4·74	5·4	427
5	0·70	0·18	4·74	6·2	511
6	0·71	0·16	4·74	5·6	499
7	0·76	0·12	4·74	5·3	462
8	0·77	0·11	4·74	5·5	479
9	0·68	0·20	4·74	5·2	513
10	0·71	0·16	4·74	5·6	518
11	0·67	0·17	5·70	4·6	494

modelled KF crystals do not touch the edges of the sample volume, 534 of which are modelled from more than one section. Best-fit ellipsoids of 247 KF phenocrysts spanning more than two sections were created in GOCAD (Figs 5e–g and 6, see also the Electronic Appendices). Their principal axes (short, intermediate, long) were manually measured in GOCAD and taken as an approximation of crystal shape. The axial ratios are

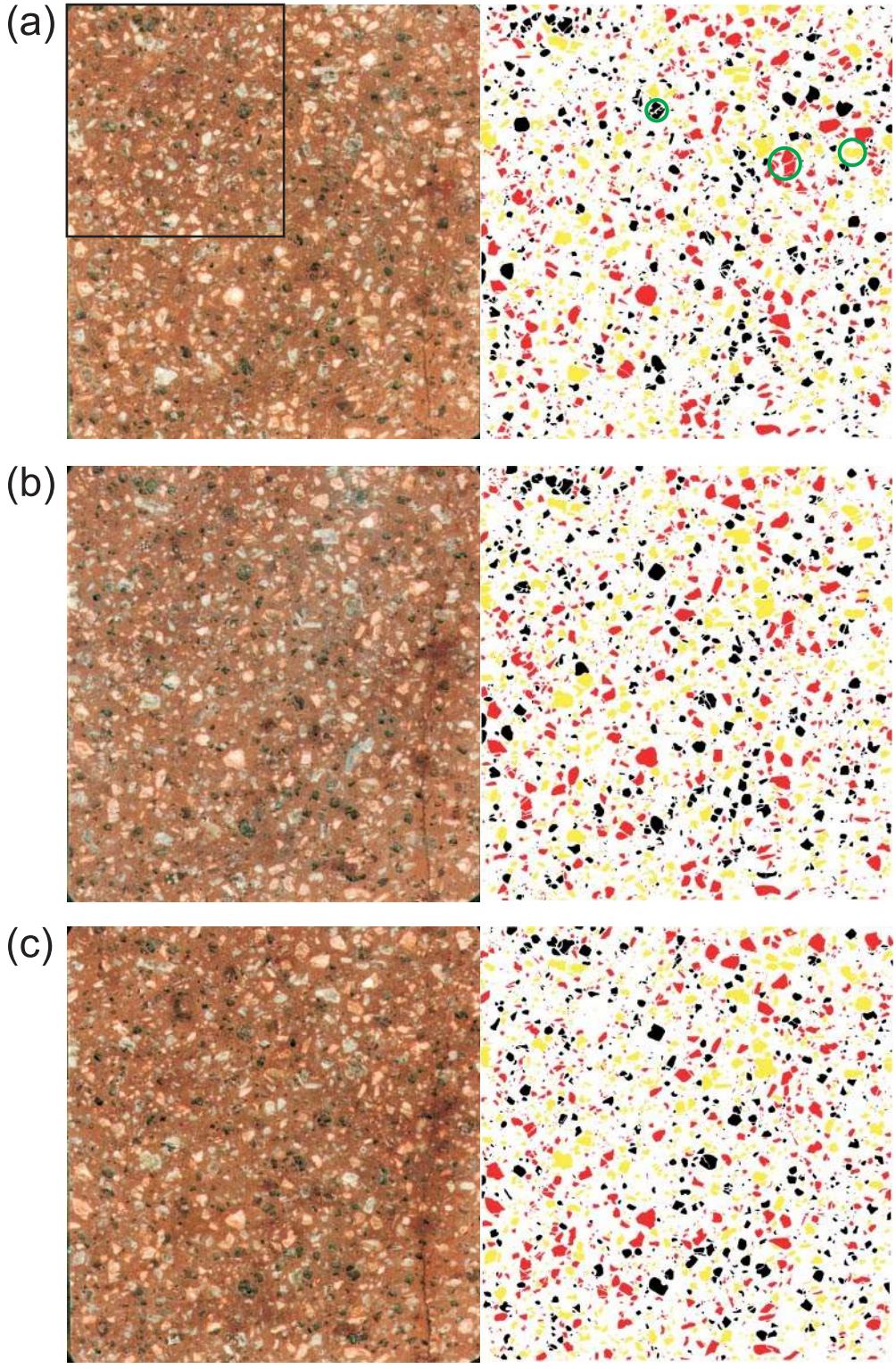

Fig. 2. (a–c) Images of three sample slabs (sections 9, 10 and 11; left) and classified images of these slabs (right). Red, K-feldspar; yellow, plagioclase; black, quartz. Edge length, ~7·5 cm. Approximate boundary of the 3D model is indicated in (a). Broken phenocrysts with very closely spaced fragments are indicated by green circles in (a).

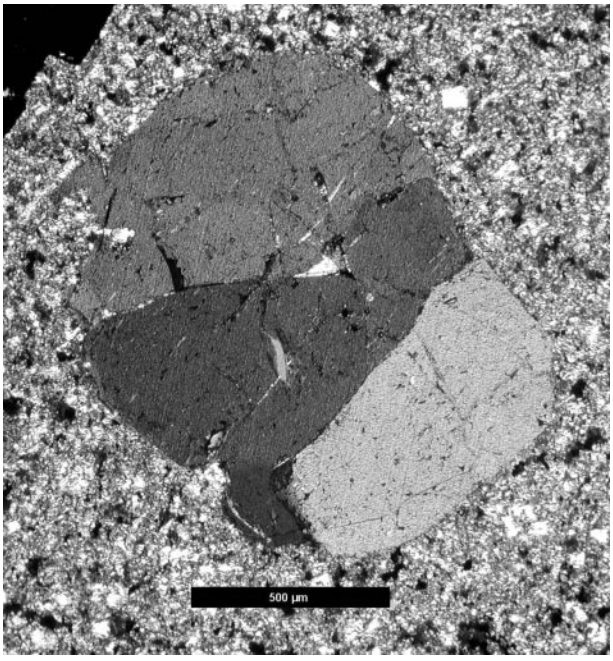

Fig. 3. Example of a broken and subsequently annealed quartz phenocryst from the Petersberg laccolith (thin-section, crossed polarized light; scale bar represents 500 µm).

plotted in a Zingg (1935) diagram to show the distribution and variation of crystal shapes (Fig. 7). The resultant model of the KF phenocrysts was then cut by 14 parallel, virtual planes, oriented at a low angle to the eroded plane to create synthetic images of K-feldspar sections for comparison with the results from the actual sections. These virtual sections were analysed in the same way as described above.

3D MODEL OF PHENOCRYSTS

True 3D crystal lengths and shapes

Crystal shapes in 3D are defined by triangulated surfaces (∗.*ts*-files in GOCAD), where each crystal is defined by a series of coordinates for nodes at the corner of each triangle constituting the surface (Fig. 4). The 3D model (Fig. 5 and the Electronic Appendix) shows that phenocrysts do not form a touching framework. More importantly, individual crystals modelled from more than two intersections exhibit complicated irregular shapes (Figs 5 and 6). These deviate considerably from crystal shapes expected when phenocrysts grow freely in a melt and, therefore, also deviate from ideal geometrical shapes so far employed in stereological CSD correction.

Figure 6 shows representative shapes for five KF phenocrysts, with their grain size (length) and aspect ratios calculated using the best-fit ellipsoid function in GOCAD (see Fig. 5 and the Electronic Appendix for an impression of section planes). Based on 247 measured

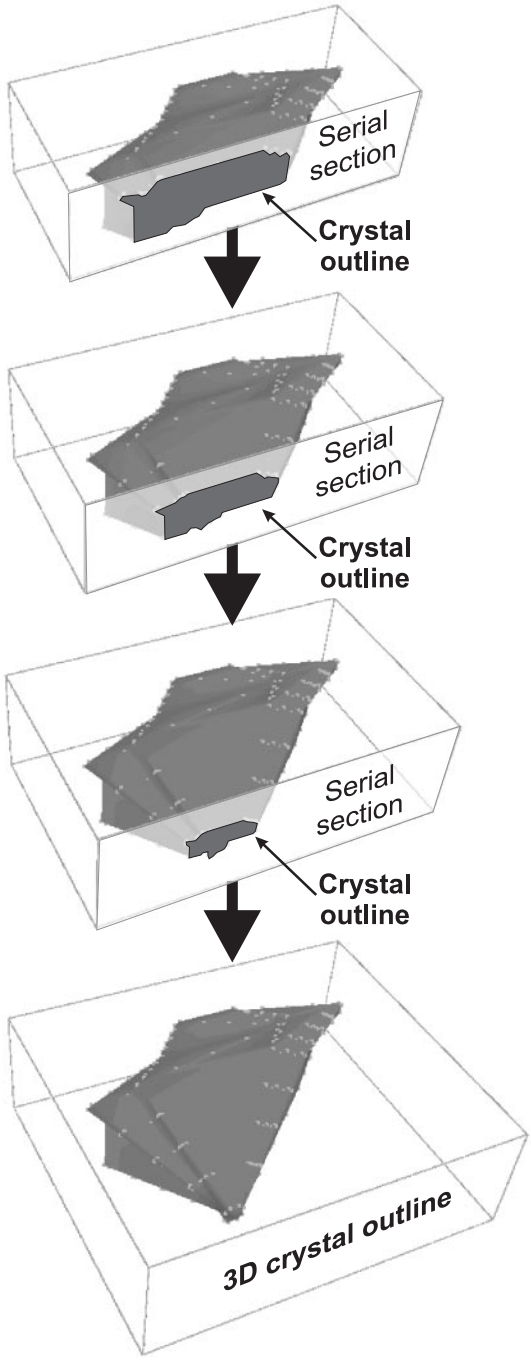

Fig. 4. Crystals are reconstructed by linking their outlines between different sections and then rendered to a 3D surface.

best-fit ellipsoids, KF crystals have a median axial ratio of 2·8:1·6:1. However, the shape distribution shows a large variation in a Zingg diagram (Fig. 7). Shapes vary considerably, from equant shapes very close to 1:1:1 to slightly elongate shapes of 5:2·3:1; examples in Fig. 6 vary from 1·7:1·5:1 to 3·3:1·9:1. Highly acicular shapes up to >10:2:1 occur for some crystals modelled

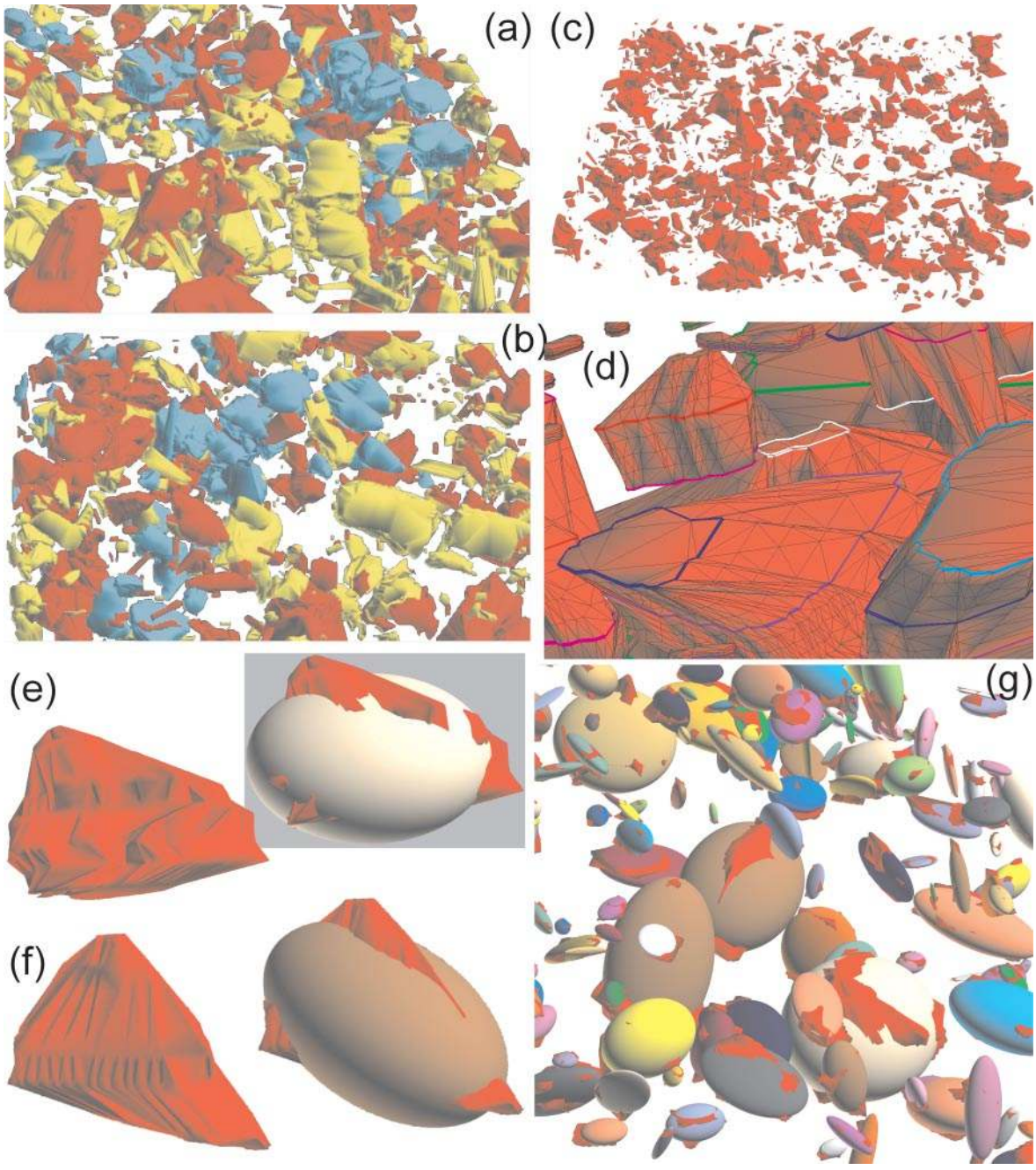

Fig. 5. (a and b) 217 reconstructed phenocrysts in a small sample volume. Yellow, PL; red, KF; light blue, QZ. Oblique (a) and top-down views (b). (c) Oblique 3D view of the model of 1599 KF phenocrysts. (d) Close-up of model of KF showing individual sections in different colours and borders of triangles calculated by GOCAD as thin black lines. Note crystals from singular sections in upper left corner. (e and f) Two reconstructed KF phenocrysts with complicated shapes reconstructed from more than two sections. Position of sections can be seen from breaks in slope on the surfaces (left). KF phenocrysts with their best-fit ellipsoids constructed with a function incorporated in GOCAD (right). (e) consists of two closely spaced fragments and has a long axis of ~2 mm, (f) of ~1 mm. (g) 247 K-feldspar phenocrysts and their best-fit ellipsoids. These images can be examined as animations in the Electronic Appendix (available at http://www.petrology.oupjournals.org).

from only two intersections. This complex arrangement of shapes is not restricted to size in terms of crystal length, but may be restricted by overall crystal volume; however, smaller-volume phenocrysts display both tabular and acicular shapes. This raises a number of issues regarding conditions of crystal growth and interpretation of the CSD produced (see subsequent discussion).

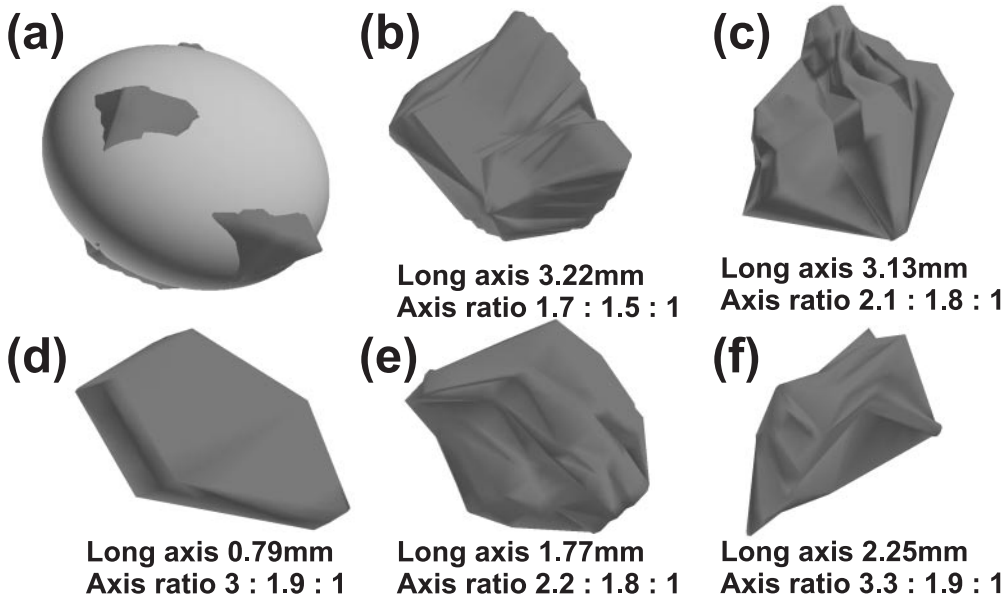

Fig. 6. Examples of the shape variation displayed by KF phenocrysts in the 3D model. (a) The shape characteristics are determined by the best-fit ellipsoid function in GOCAD. (b–f) Five examples of phenocrysts showing their maximum dimension and the principal axes of their best-fit ellipsoids. Position of section planes can be estimated by breaks in slope on the surfaces.

To calculate the true 3D long axis of each crystal, a program was written to extract *xyz*-coordinates defining each crystal from the ∗.*ts*-files, and then to calculate the longest distance between these points, defining this as the crystal's long axis (length). From these data, CSD_{3D} can be plotted (Fig. 7) and compared with stereologically corrected CSD_{2D}. CSD_{3D} is characterized by a simple straight slope with a gradient of −1·02, corresponding to a CL of 0·98 mm, an intercept of −1·36 corresponding to a final nucleation density of 0·23 mm^{-4} and a regression coefficient of 0·99 (only unfilled data points used for regression analysis). CSD_{3D} excluding crystals modelled from singular sections is not significantly different from CSD_{3D} with all modelled crystals. Gradients differ by only 0·05; however, the singular sections extend the dataset to considerably smaller crystal sizes (Fig. 7).

Testing reproducibility of CSD at different sample volumes

Representative sample size is an important question in conjunction with the quantification of crystal populations, i.e. at what sample size is the texture of the sample characteristic of a larger portion of the rock? Additionally, the sample must be large enough to obtain a statistically valid quantification of the crystal population. This is especially important when small-scale variations in rock texture are to be quantified. 3D sphere models of different size distributions have been developed which can be sectioned to produce reference textures in 2D (Jerram, 1996, 2001). Grain size distributions measured on these models and similar models of low- to medium-aspect ratio prisms produce accurate results when >300 individuals are measured (Jerram, 1996). As a comparison with previous studies based on synthetic 3D models, the large sample size of the 3D model presented in this study is ideal to test the minimum sample size required to correctly measure CSD_{3D}. Figure 8 shows CSD plots for different sample volumes of the model. The CSD starts to break down between 9/64 (0·141) and 1/9 (0·111) of the original sample size, which relates to between 224 and 178 crystals. This result suggests that sample sizes of greater than ∼200 are required to accurately reproduce the CSD in this study and will act as a guide for other studies using CSD data.

Comparing 3D and 2D CSDs

$CSD_{3D,cor}$ of KF, PL and QZ in all sections are presented in Fig. 9. They are all very well defined straight lines (average regression coefficients R^2 are 0·98 for all phases). Small-size data points were not included in calculating R^2 because of the large errors in stereological correction (Higgins, 2000). The CSDs of the two feldspars (KF, PL) are very similar (average slopes of −1·16 and −1·17; intercepts of −1·2 and −1·1; maximum size ∼11 mm), QZ has steeper slopes and smaller maximum sizes (−1·4, −1·7, 7 mm; Table 2).

Figure 10 shows interpretative plots for CSDs [characteristic length (CL ∼ CSD slope) vs modal abundance]. CL varies by ∼0·6 mm from section to section. In Figs 10 and 11, three slabs from the original

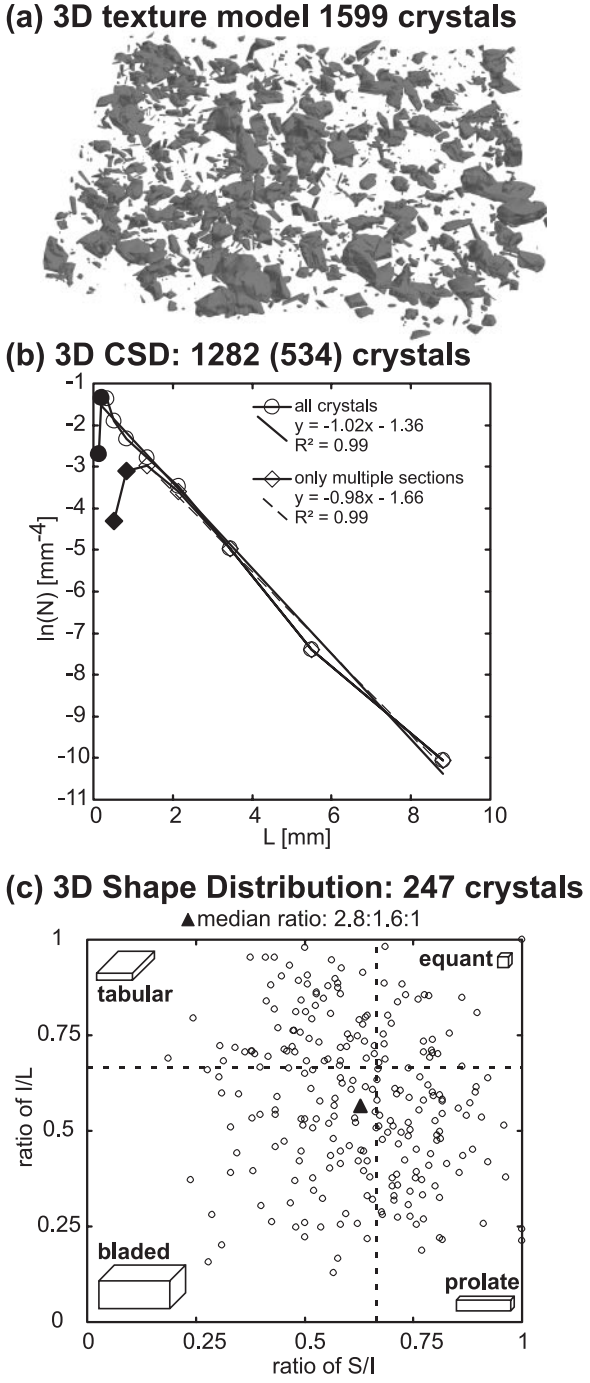

Fig. 7. (a) 3D reconstruction of KF phenocrysts with 1599 crystals; (b) resultant CSD_{3D} plot of crystal population (1282 individual KF phenocrysts) using longest distances between nodes of crystals' surfaces. Crystals touching the edges of the sample volume are excluded. The CSD excluding crystals modelled from only one section is also shown to illustrate the validity of the procedure applied in this study. Filled data points were not included in regression analysis. (c) Shape distribution of 247 KF phenocrysts in the 3D model. Ratios of intermediate (I) over long (L) and short (S) over intermediate (I) axes are plotted on a Zingg diagram (Zingg, 1935) to indicate particular crystal geometries. Axes measured manually in GOCAD from best-fit ellipsoids created (compare Fig. 5). (Note very large variation of shapes.)

larger sample (90499) have higher CL and modal abundances than individual serial sections, but agree very well with the CL of the CSD_{3D} [with standard errors calculated from sample set of Mock *et al.* (2003)]. According to the standard errors, the variation in modal abundance seems to be larger than the variation in CL in serial sections. The modal abundance of the 3D model is slightly higher than in 90499, but still falls well within the range given by individual serial sections. To determine modal abundances in the 3D model, volumes were computed from long axes according to equation (2) below, assuming ellipsoids with an aspect ratio of 2·8:1·6:1 (median ratio of 3D model) giving a sum of KF volumes of 534·6 mm^3 (3D real length in Fig. 10). Alternatively, volumes of crystals were taken as measured directly in GOCAD, giving a sum of KF volumes of 381·9 mm^3 (3D real volume in Fig. 10). Both sets of volumes were summed and related to sample volume calculated from the maximum and minimum coordinates of the modelled crystals. Thus, KF content varies between 5 and 8% in the 3D model and between 4·5 and 8·2% in individual sections. The average overall content of all felsic phenocrysts (KF, PL, QZ) determined from the sections is 16%.

Histograms of the two volume distributions of KF also show slight differences (Fig. 11). CSD_{3D} and $CSD_{3D,cor}$ of individual sections are compared in Figs 10 and 11. Real and virtual sections display a considerable spread in CL vs modal abundance plots. This convincingly illustrates the variation of quantitative textural parameters as a result of section effects (see below). In a stereological correction, CSD_{2D} is converted into $CSD_{3D,cor}$ assuming an ideal crystal shape (Higgins, 2000). Shapes used for this purpose are usually spheres, spheroids or ellipsoids with variable aspect ratios or rectangular solids with aspect ratios between equant and acicular shapes. Correction factors are also applied to take fabrics into account (i.e. preferred orientations arising from acicular crystals; Sahagian & Proussevitch, 1998; Higgins, 2000). For comparative purposes, we model 3D size distribution with volume data from 3D crystals. A linear measure of size was determined from modelled crystal volumes as (1) diameter (d) of an equal volume sphere and (2) long axis (c) of an equal volume ellipsoid with axial ratios of 2·8:1·6:1 (median ratio of 247 KF crystals). The equations used are (V = volume)

$$d_{\text{sphere}} = 2\left(\sqrt[3]{\frac{3V}{4\pi}}\right) \quad (1)$$

$$c_{\text{ellipsoid}} = 2\left(\sqrt[3]{\frac{3V}{0{\cdot}8\pi}}\right). \quad (2)$$

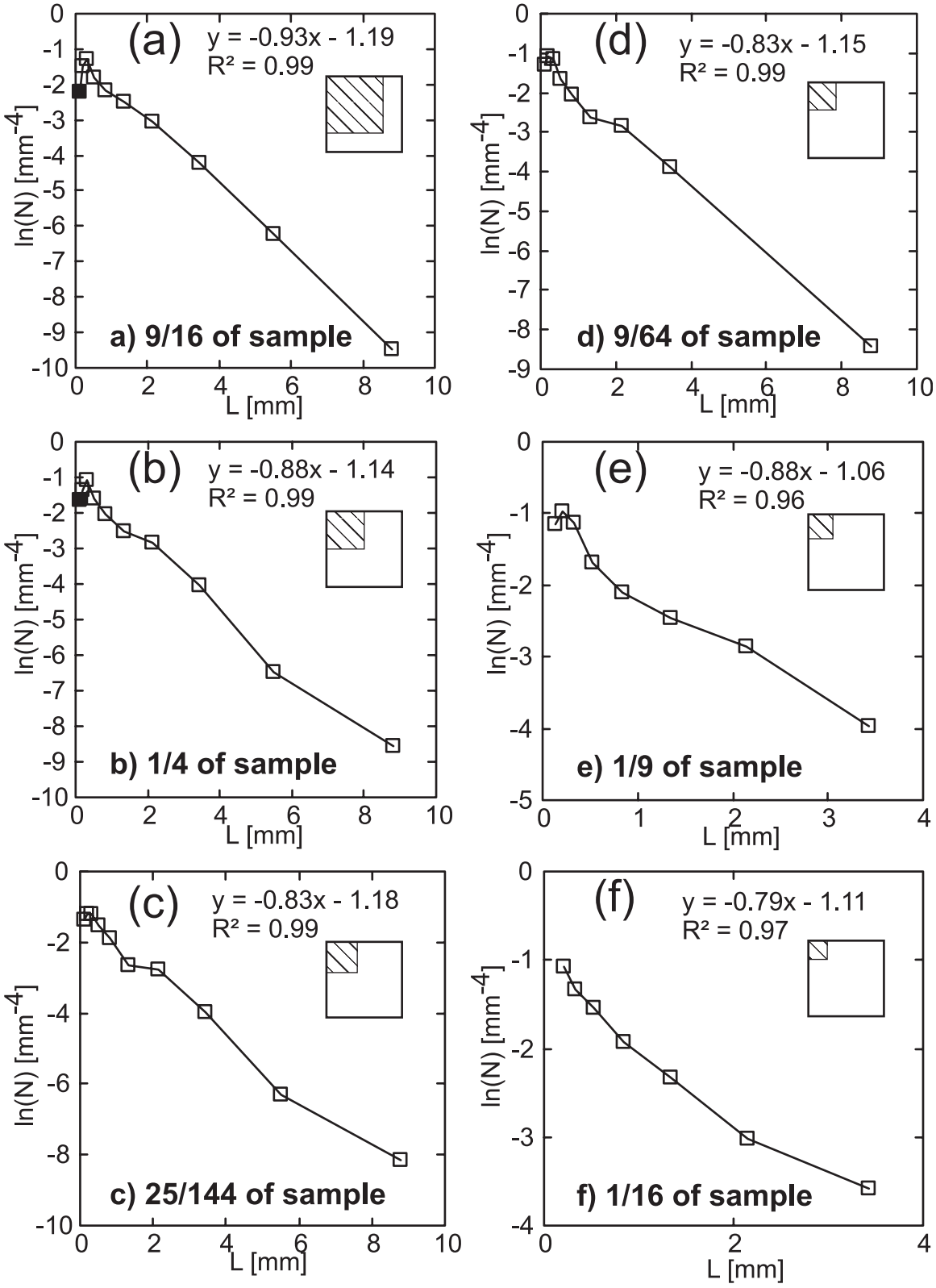

Fig. 8. Testing sample size vs robustness of CSD: (a) CSD of 9/16 (905 crystals); (b) CSD of 1/4 (424 crystals); (c) CSD of 25/144 (287 crystals); (d) CSD of 9/64 (224 crystals); (e) CSD of 1/9 (178 crystals); (f) CSD of 1/16 (88 crystals) of original sample volume.

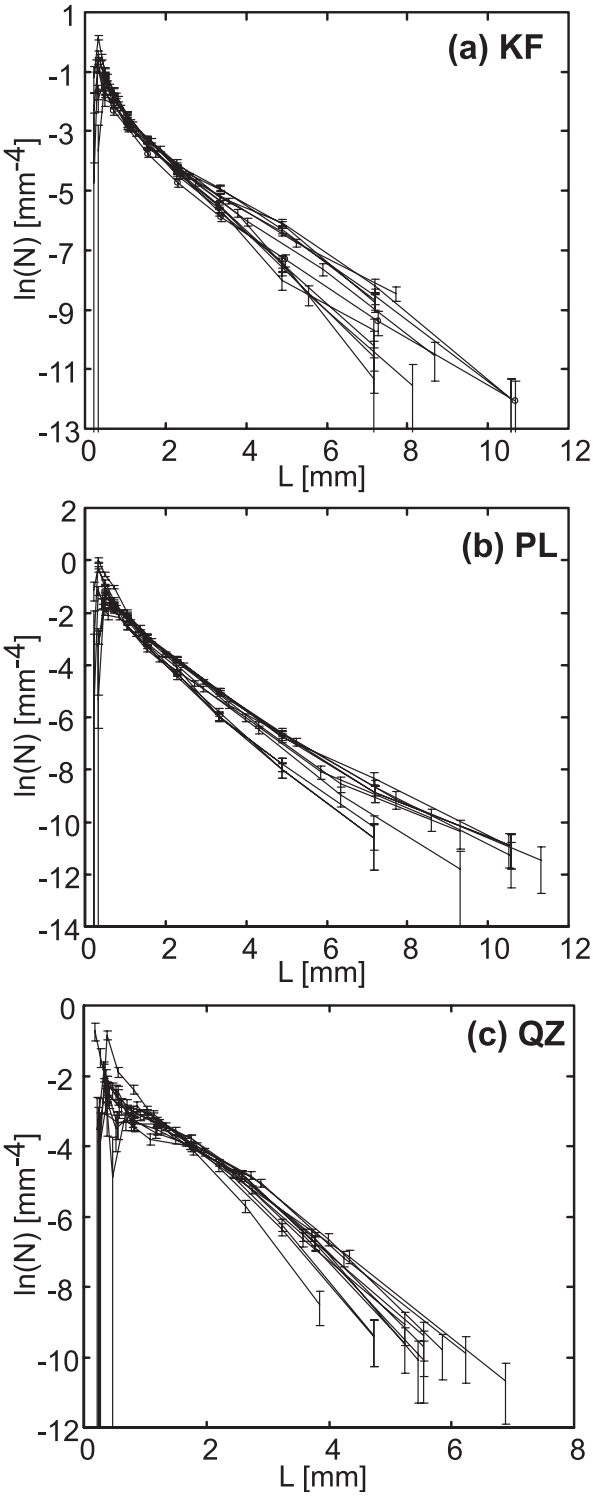

Fig. 9. CSD plots, logarithmic population density (N) vs size (L), of serial sections for (a) KF, (b) PL and (c) QZ. Error bars calculated by CSDCorrections 1.36 (Higgins, 2000). Average regression coefficients R^2 are 0·98 for all phases. The CSDs of the two feldspars (KF, PL) are very similar (average slopes of −1·16 and −1·17; intercepts of −1·2 and −1·1; maximum size ∼11 mm). QZ has a steeper slope, larger intercept and smaller maximum size (–1·4, −1·7, 7 mm).

Variation as a result of different shape models in stereology is demonstrated in Fig. 11 by CSDs for these two models in comparison with CSD_{3D}. The sphere model clearly has markedly different CSD parameters from the other models (see also Table 3). This observation makes it clear that too simple a model for stereological correction of CSDs can yield misleading results (also discussed below). The CSD_{3D} falls between the CSD of the ellipsoid model and the CSDs for the larger sample determined stereologically (Fig. 11a). Their CLs are very similar, at around 0·95 ± 0·1 mm. The intercepts, on the other hand, vary from +0·4 to −3. Model shapes also yield smaller maximum sizes, whereas, in $CSD_{3D,cor}$, maximum sizes are larger than those in CSD_{3D}.

Virtual sections through the model of KF phenocrysts have smaller CL and a wider range of modal abundances. Compared with samples from the whole Halle Laccolith Complex (Mock *et al.*, 2005), the serial sections occupy the lower part of the sample cloud. They extend to much lower modal abundances and CL (Fig. 10c).

DISCUSSION

Variability within the sample cube

Multiple sections through one crystal produce a distribution of sizes. In sections not sampling the maximum size, large crystals are, thus, removed from large size bins and introduced into small size bins, increasing the gradient of the CSD. Modal abundance is similarly affected. This effect will only influence CSDs in closely spaced sections through a rock sample if crystals are unevenly distributed in the sample, e.g. by granular sorting of crystals under shear (Petford & Koenders, 2001, 2003; Mock *et al.*, 2003). In sections of randomly distributed crystals, the above effects would cancel out.

Small sections of large crystals become part of a large crystal in the 3D model and populate large size bins in CSD_{3D} and not small size bins, as in $CSD_{3D,cor}$, hence the larger CL of the 3D model than of its individual sections. The virtual sections through the 3D model show a larger variation in CSD parameters than the real sections (Fig. 10). This might reflect their higher number (14) and slightly different orientation. They do not vary significantly from the real sections, though. The latter fall into two groups: one with uniform CL and modal abundances, and one whose modal abundances vary by ∼1–2% and whose CLs are larger by ∼0·2 mm (Fig. 10). The members of these groups are not distributed uniformly through the sectioned sample volume. This variation pattern might stem from the presence of flow structures formed by granular flow sorting (see above), assuming sections were oriented close to parallel to them. However, if the spacing of the sections is considered, this becomes less likely, because the CL of the phenocrysts is

larger than the section spacing and the maximum size spans almost the entire sectioned thickness.

2D–3D correction

Stereologically corrected CSDs of the sections reproduce CSD_{3D} within reasonable error (~10% for CL, ~20% for maximum lengths and higher variability for intercepts; Fig. 10). Thus, even for non-crystallographic shapes, application of stereological correction methods for CSD analysis using idealized shapes seems to be justified to a first approximation, but care should be taken in further interpretations (see below).

CSD correction has to take into account the higher probability of intersecting large grains than smaller grains in any random section. Furthermore, any random section through a rock texture probably produces a section for each individual grain smaller than its true size in three dimensions (see above). Thirdly, preferred orientation of crystals, especially ones with high aspect ratios, makes CSD_{2D} strongly dependent on the orientation of the section. These problems have been termed dimension shift, shape and orientation problem or cut section effect and intersection probability or big grain effect, and have been solved for a number of simple model shapes (Jerram, 1996; Peterson, 1996; Sahagian & Proussevitch, 1998; Higgins, 2000).

The problem of more complicated shapes than spheres, either simple prolate and oblate ellipsoids or rectangular solids with varying aspect ratios, however, has not been solved analytically. This study has shown an abundance of non-crystallographic shapes of crystals in rocks, even under the assumption of uninhibited growth from a melt. It has also highlighted problems of having crystals with markedly different 3D shapes within the same population. Furthermore, the phenocrysts in this study do not form a shape fabric as a result of alignment of acicular or platy crystals. The complicated shapes of reconstructed crystals in this study, however, have important implications for assumed models of crystal growth, especially in the light of simple, straight CSDs.

Crystal growth and crystal shapes

Crystal growth processes in petrology have been modelled extensively (Spohn *et al.*, 1988; Hort & Spohn, 1991; Toramaru, 2001), although comprehensive models for the complex multicomponent systems of silicate magmas have not been developed. Qualitative results and order-of-magnitude calculations accounting for differences between volcanic and plutonic textures are available. Nevertheless, it has been shown what kind of size distributions will be generated during simple crystallization of magma (Marsh, 1998). Of special importance for the evolution of an igneous texture is the consideration of the processes that add to simple nucleation and growth, e.g. crystal growth by annexation of small crystals into large ones (after abutment of crystals) by grain boundary diffusion, producing optically continuous large crystals. These processes often produce kinked or concave-up CSDs resembling fragmented size distributions. Curved CSDs, however, are not observed in the data presented here.

Kile & Eberl (2003) proposed two crystal growth laws: size-dependent (proportionate) and size-independent (disproportionate) growth. In proportionate growth, the relative size difference among crystals remains constant, e.g. size differs by a factor of two; in disproportionate growth, growing crystals keep the same absolute difference in size, e.g. 100 μm. Proportionate crystal growth produces log-normal CSDs like those frequently found in natural systems. Conventional models for CSD often assume disproportionate growth, which is not confirmed in experiments. On the other hand, reactant supply by advection has been found to control proportionate growth, whereas disproportionate growth is controlled by diffusive reactant supply. In felsic magmas, advection might not play an important role in supplying growing crystals with components because of the very high magma viscosities. Thus, by draining away crystal components from the vicinity of phenocrysts, ideal crystallographic shapes might develop into complex shapes by differential (phase-dependent) anisotropic (direction-dependent) overgrowth and resorption. Furthermore, controlling mechanisms on crystal growth are more complex in natural systems than in experiments. Other parameters influence crystal growth (Dowty, 1980), such as:

- the abundance of suitable sites for the attachment of molecules on crystal faces;
- crystallographic twins providing re-entrant angles that are favourable sites for the attachment of new molecules;
- rate-limited diffusion of reactants towards, and gradient-limited diffusion of heat away from, the crystal;
- adsorption of foreign atoms inhibiting growth;
- the overall growth mechanism being interface-controlled vs diffusion- or heat-controlled growth or continuous vs layer growth controlled by the abundance and rates of surface nucleation, twins, screw dislocations, etc.

In addition to indicating crystal growth processes, the CSDs of crystal populations can be used to determine residence times of crystals in a magmatic system. CSD slope is proportional to the product of growth rate and residence time in an open system (Marsh, 1998). It is also significantly influenced by the model shape applied during stereological correction. All other parameters being equal and constant, residence times for simple sphere models are calculated to be twice as long as those for

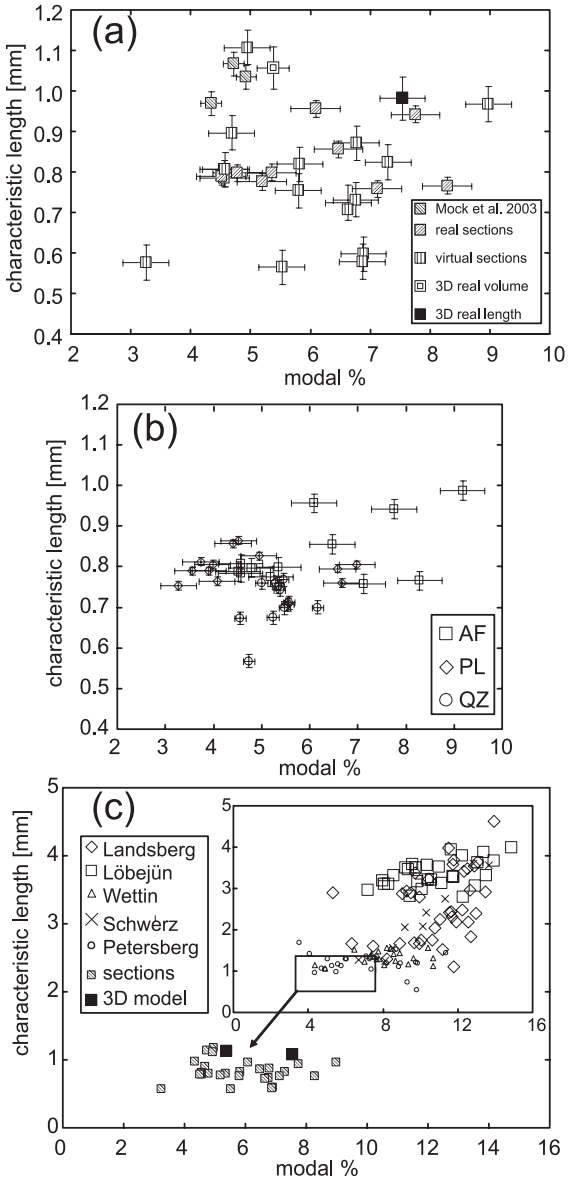

Fig. 10.(a) Characteristic length vs modal abundance plot for serial sections for KF phenocrysts. Data from real 2D sections corrected after Higgins (2000), 14 virtual sections through the 3D model, three sample slabs (90499) from Mock *et al.* (2003) and the 3D model itself (size calculated from coordinates of nodes and from volumes as long axis of equal volume ellipsoid with median aspect ratio of shape distribution, Fig. 7c). (See text for the calculation of modal abundances for 3D real volume and 3D real length.) (b) Characteristic length (CL) vs modal abundance of all three felsic phenocryst phases from the real serial sections. (c) Comparison of serial sections with CSDs from the whole laccolith complex (Mock *et al.*, 2005) in a plot of CL vs modal abundance. Error bars in (a) and (b) are standard errors (SE) calculated from the corresponding datasets mentioned in (a), using

$$SE = \sqrt{\frac{\sum_{i=1}^{n} y_i^2}{(n-1)(n)}}$$

where y_i is the ith datum in the dataset and n is the number of data points in the dataset.

measured 3D size data (Table 3). Different growth rates assumed for calculation of residence times reflect the range of growth rates determined for silicate systems from experiment and numerical modelling (Swanson, 1977; Lasaga, 1982; Spohn *et al.*, 1988; Cashman, 1993). Additionally, CSD intercepts (final nucleation density) vary for different model shapes (Table 3).

In summary, the complicated shapes found in the 3D model of felsic phenocrysts stem from a complex interplay of anisotropic growth mechanisms in connection, most probably, with variable growth laws, resorption and fracturing of crystals, whereas the CSDs (Fig. 6) as an integration of these processes do not indicate complexity.

Touching frameworks of crystals in magmas

The development of touching frameworks of crystals in magmas has been shown to depend strongly on the crystal volume fraction, shape and fabric (Saar *et al.*, 2001, and references therein). Critical volume fractions for touching frameworks range from 0·08 to 0·2 for a variety of shapes (Saar *et al.*, 2001). Quantification of spatial distribution patterns of crystals in comparison with modal abundances can also provide a threshold for touching vs non-touching crystal populations (Jerram *et al.*, 2003). The spatial distribution pattern of the 3D model presented here will be discussed elsewhere. A similar threshold value to that of Saar *et al.* (2001) for the formation of a touching framework of phenocrysts has been verified by basalt melting experiments (Philpotts *et al.*, 1998). Moreover, clusters of crystals can be viewed as essential building blocks of any igneous rock. These crystal clusters are much more likely to connect into a 3D touching framework at lower crystal abundances than individual crystals (Jerram *et al.*, 2003). In contrast, phenocrysts in the 3D model presented here are generally randomly distributed, do not form crystal clusters (Mock *et al.*, 2003) and clearly do not form a touching framework. Additionally, the aspect ratios of the phenocrysts in this study are, in general, not acicular and the modal abundances just reach the critical values found in the models of Saar *et al.* (2001). Thus, it is suggested that phenocrysts, especially in silicic magmas, can sustain non-touching frameworks up to a slightly higher volume fraction than those referred to above. The higher yield strength of the rhyolitic melt might allow phenocrysts to be suspended without interconnection.

CONCLUSIONS AND OUTLOOK

This study has investigated the true 3D size and shape distributions of felsic phenocrysts in a highly porphyritic, rhyolitic laccolith from the HVC, Germany. Rigorous 3D reconstruction of populations of felsic crystals using

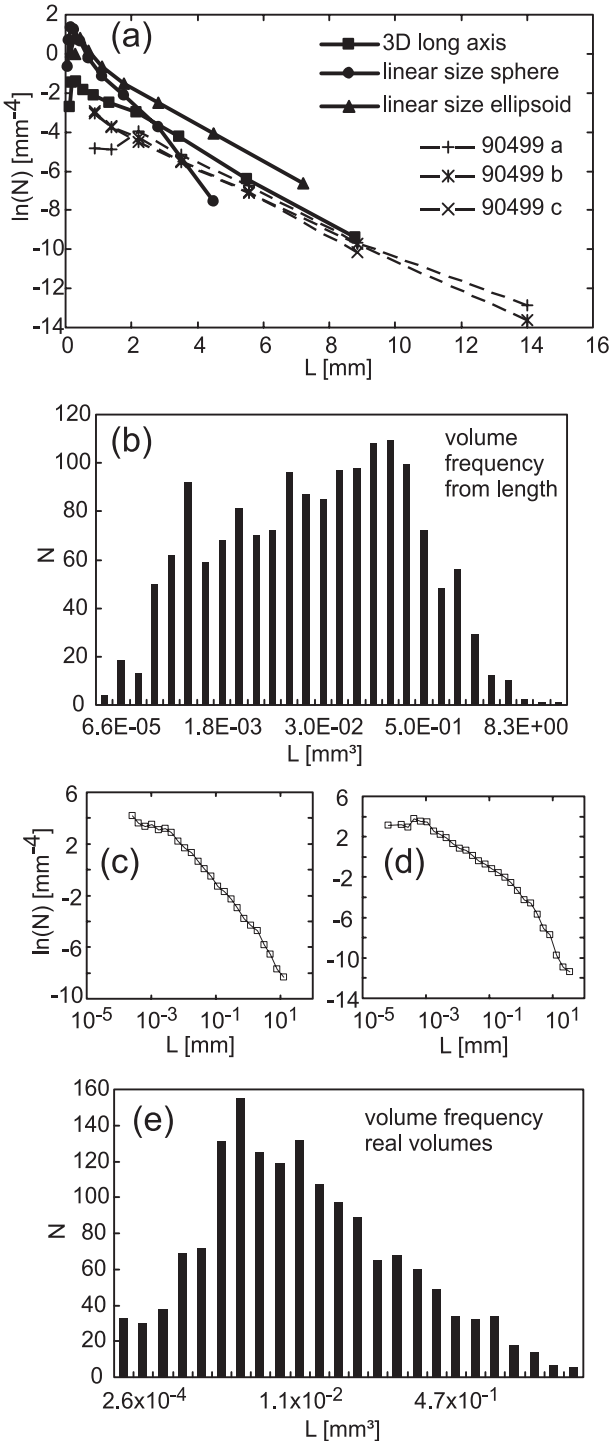

Fig. 11. (a) CSD plots of linear sizes calculated from coordinates and from volumes of KF phenocrysts in the 3D model [diameter of equal volume sphere, long axis of equal volume ellipsoid, equations (1) and (2)] and comparison with three sample slabs of sample 90499 from Mock *et al.* (2003). (b–e) Crystal volume distribution of KF in the 3D model. (b) Histogram of volume frequency calculated from lengths [equation (2)]. (c) CSD plot from (b). (d) CSD plot of (e); (e) shows histogram of volume frequency calculated from measured volumes (compute-volume function of GOCAD).

Table 3: Influence of shape on time-scale calculations using CSD

	Sphere	Ellipsoid	3D length	Growth rate (cm/s)
Slope	−1·84	−1·01	−0·88	
Growth rate × res. time	0·55	0·99	1·13	
Intercept	1·03	0·40	−1·45	
Res. time 1 (days)	2·1	3·8	4·4	$3{\cdot}0 \times 10^{-6}$
Res. time 2 (weeks)	18·0	32·6	37·4	$5{\cdot}0 \times 10^{-8}$
Res. time 3 (years)	1727	3131	3595	$1{\cdot}0 \times 10^{-11}$

Different growth rates reflect the range of growth rates determined for silicate systems from experiment and numerical modelling (Swanson, 1977; Lasaga, 1982; Spohn *et al.*, 1988; Cashman, 1993); res, residence.

serial grinding techniques along with quantification of textures using 3D visualization software has allowed the following conclusions and recommendations:

(1) CSD_{3D} agrees well with stereologically corrected size distributions determined from 2D sections, but individual sections used for the reconstruction show considerable scatter in the parameters of $CSD_{3D,cor}$.
(2) The spatial characteristics of 3D populations indicate a non-touching framework, which confirms previous interpretations based on 2D spatial distribution analysis (Jerram *et al.*, 2003; Mock *et al.*, 2003). The threshold volume fraction established for formation of touching frameworks by numerical models might be higher in natural—especially silicic—rocks.
(3) A marked difference in shape characteristics of crystals of different sizes within the same population was detected. This indicates changing crystallization conditions during crystal growth. This fact is not mirrored in the relatively straight CSDs normally interpreted as a product of simple nucleation and growth histories. Thus, simple CSDs are not necessarily an indicator of simple crystallization conditions.
(4) CSD_{3D} data can be robustly reproduced from sample sizes greater than ~200 individual crystals.
(5) Crystal shapes assumed during stereological correction of CSD data have a major influence on time-scales of crystallization calculated from CSD slopes.

ACKOWLEDGMENTS

B.-C. Ehling and the Landesamt für Geologie und Bergwesen Sachsen-Anhalt are thanked for providing the sample. M. Magnus is thanked for preparation of

the sample and assistance with serial erosion. J. Neff, T. Lohr and other student assistants at Technische Universität Bergakademie Freiberg are thanked for help with image classification. C. Bauer helped in converting classified images into shape files. M. Apel, G. van den Boogaart and R. Single are thanked for help with GOCAD. C. Breitkreuz, D. Morgan and J. Day made insightful and helpful comments on earlier versions of the manuscript. B. Marsh, M. Higgins and an anonymous reviewer are thanked for their reviews. This study was undertaken while A.M. was employed within a Deutsche Forschungsgemeinschaft project granted to C. Breitkreuz (Br 997/18–1,2) at Technische Universität Bergakademie Freiberg, Germany.

SUPPLEMENTARY DATA

Animations of Fig. 5a–g (Animations 1–6) are available as supplementary data on *Journal of Petrology* online.

REFERENCES

Best, M. G. & Christiansen, E. H. (1997). Origin of broken phenocrysts in ash-flow tuffs. *Geological Society of America Bulletin* **109**, 63–73.

Breitkreuz, C. & Kennedy, A. (1999). Magmatic flare-up at the Carboniferous/Permian boundary in the NE German Basin revealed by SHRIMP zircon ages. *Tectonophysics* **302**, 307–326.

Breitkreuz, C. & Mock, A. (2004). Are laccolith complexes characteristic of transtensional basin systems? Examples from Permo-Carboniferous Central Europe. In: Petford, N. & Breitkreuz, C. (eds) *Physical Geology of High-level Magmatic Systems*. *Geological Society, London, Special Publications* **234**, 13–31.

Bryon, D. N., Atherton, M. P. & Hunter, R. H. (1995). The interpretation of granitic textures from serial thin sectioning, image analysis and three-dimensional reconstruction. *Mineralogical Magazine* **59**, 203–211.

Cashman, K. V. (1993). Relationship between plagioclase crystallization and cooling rate in basaltic melts. *Contributions to Mineralogy and Petrology* **113**, 126–142.

Cashman, K. V. & Marsh, B. D. (1988). Crystal Size Distribution (CSD) in rocks and the kinetics and dynamics of crystallization II: Makaopuhi lava lake. *Contributions to Mineralogy and Petrology* **99**, 292–305.

Castro, J. M., Cashman, K. V. & Manga, M. (2003). A technique for measuring 3D crystal-size distributions of prismatic microlites in obsidian. *American Mineralogist* **88**, 1230–1240.

Cooper, K. M. & Reid, M. R. (2003). Re-examination of crystal ages in recent Mount St. Helens lavas: Implications for magma reservoir processes. *Earth and Planetary Science Letters* **213**, 149–167.

Cooper, M. R. & Hunter, R. H. (1995). Precision serial lapping, imaging and three-dimensional reconstruction of minus-cement and post-cementation intergranular pore-systems in the Penrith Sandstone of north-western England. *Mineralogical Magazine* **59**, 213–220.

Delesse, M. A. (1848). Procédé mécanique pour déterminer la composition des roches. *Annales des Mines* **13**, 379–388.

Denison, C. & Carlson, W. D. (1997). Three-dimensional quantitative textural analysis of metamorphic rocks using high-resolution computed X-ray tomography: Part II—Application to natural samples. *Journal of Metamorphic Geology* **15**, 45–57.

Denison, C., Carlson, W. D. & Ketcham, R. A. (1997). Three-dimensional quantitative textural analysis of metamorphic rocks using high-resolution computed X-ray tomography: Part I—Methods and techniques. *Journal of Metamorphic Geology* **15**, 29–44.

Dowty, E. (1980). Crystal growth and nucleation theory and the numerical simulation of igneous crystallization. In: Hargraves, R. B. (ed.) *The Physics of Magmatic Processes*. Princeton, NJ: Princeton University Press, pp. 419–485.

Eigenfeld, F. & Schwab, M. (1974). Zur geotektonischen Stellung des permosilesischen subsequenten Vulkanismus in Mitteleuropa. *Zeitschrift für Geologische Wissenschaften* **2**, 115–137.

Elias, H. & Hyde, D. M. (1983). *A Guide to Practical Stereology*. Basel: Karger.

Hammer, J. E., Cashman, K. V., Hoblitt, R. P. & Newman, S. (1999). Degassing and microlite crystallization during pre-climactic events of the 1991 eruption of Mt. Pinatubo, Philippines. *Bulletin of Volcanology* **60**, 355–380.

Hammer, J. E., Cashman, K. V. & Voight, B. (2000). Magmatic processes revealed by textural and compositional trends in Merapi dome lavas. *Journal of Volcanology and Geothermal Research* **100**, 165–192.

Herbert, M. J. & Jones, C. B. (2001). Contour correspondence for serial section reconstruction: Complex scenarios in palaeontology. *Computers and Geosciences* **27**, 427–440.

Higgins, M. D. (1996). Magma dynamics beneath Kameni Volcano, Thera, Greece, as revealed by crystal size and shape measurements. *Journal of Volcanology and Geothermal Research* **70**, 37–48.

Higgins, M. D. (2000). Measurement of crystal size distributions. *American Mineralogist* **85**, 1105–1116.

Higgins, M. D. (2002). Closure in crystal size distribution (CSD), verification of CSD calculations and the significance of CSD fans. *American Mineralogist* **87**, 160–164.

Higgins, M. D. & Roberge, J. (2003). Crystal size distribution of plagioclase and amphibole from Soufrière Hills Volcano, Montserrat: Evidence for dynamic crystallization–textural coarsening cycles. *Journal of Petrology* **44**, 1401–1411.

Hort, M. & Spohn, T. (1991). Numerical simulation of the crystallization of multicomponent melts in thin dikes or sills—2: Effects of heterocatalytic nucleation and composition. *Journal of Geophysical Research* **96**, 485–499.

Jerram, D. A. (1996). The development and application of detailed textural analysis techniques. A case study: the origin of komatiite cumulates. PhD, University of Liverpool.

Jerram, D. A. (2001). Visual comparators for degree of grain-size sorting in two and three-dimensions. *Computers and Geosciences* **27**, 485–492.

Jerram, D. A. & Cheadle, M. J. (2000). On the cluster analysis of grains and crystals in rocks. *American Mineralogist* **85**, 47–67.

Jerram, D. A., Cheadle, M. C. & Philpotts, A. R. (2003). Quantifying the building blocks of igneous rocks: Are clustered crystal frameworks the foundation? *Journal of Petrology* **44**, 2033–2051.

Ketcham, R. A. & Carlson, W. D. (2001). Acquisition, optimization and interpretation of X-ray computed tomographic imagery: Applications to the geosciences. *Computers and Geosciences* **27**, 381–400.

Kile, D. E. & Eberl, D. D. (2003). On the origin of size-dependent and size-independent crystal growth: Influence of advection and diffusion. *American Mineralogist* **88**, 1514–1521.

Kuscu, G. G. & Floyd, P. A. (2001). Mineral compositional and textural evidence for magma mingling in the Saraykent volcanics. *Lithos* **56**, 207–230.

Lasaga, A. C. (1982). Toward a master equation in crystal growth. *American Journal of Science* **282**, 1264–1288.

Lorenz, V. & Nicholls, I. A. (1984). Plate and intraplate processes of Hercynian Europe during the Late Paleozoic. *Tectonophysics* **107**, 25–56.

Mallet, J.-L. (1992). Discrete smooth interpolation in geometric modelling. *Computer Aided Design* **24**, 178–191.

Marschallinger, R. (1998). A method for three-dimensional reconstruction of macroscopic features in geological materials. *Computers and Geosciences* **24**, 875–883.

Marsh, B. D. (1988). Crystal size distribution (CSD) in rocks and the kinetics and dynamics of crystallization: I—Theory. *Contributions to Mineralogy and Petrology* **99**, 277–291.

Marsh, B. D. (1998). On the interpretation of crystal size distributions in magmatic systems. *Journal of Petrology* **39**, 553–599.

Mock, A., Jerram, D. A. & Breitkreuz, C. (2003). Using quantitative textural analysis to understand the emplacement of shallow level rhyolitic laccoliths: A case study from the Halle volcanic complex, Germany. *Journal of Petrology* **44**, 833–849.

Mock, A., Ehling, B.-C. & Breitkreuz, C. (2005). Anatomy of a laccolith complex: Geometry and texture of porphyritic rhyolites in the Permocarboniferous Halle Volcanic Complex (Germany). *Neues Jahrbuch für Geologie und Paläontologie Abhandlungen* (in press).

Peterson, T. D. (1996). A refined technique for measuring crystal size distribution in thin section. *Contributions to Mineralogy and Petrology* **124**, 395–405.

Petford, N. & Koenders, M. A. (2001). Consolidation phenomena in sheared granitic magma: Effects of grain size and tortuosity. *Physics and Chemistry of the Earth (A)* **26**, 281–286.

Petford, N. & Koenders, M. A. (2003). Shear-induced pressure changes and seepage phenomena in a deforming porous layer: I. *Geophysical Journal International* **155**, 857–869.

Petford, N., Davidson, G. & Miller, J. A. (2001). Investigation of the petrophysical properties of a porous sandstone sample using confocal scanning laser microscopy. *Petroleum Geoscience* **7**, 99–105.

Philpotts, A. R., Shi, J. Y. & Brustman, C. M. (1998). Role of plagioclase crystal chains in the differentiation of partly crystallized basaltic magma. *Nature* **395**, 343–346.

Randolph, A. D. & Larson, M. A. (1988). *Theory of Particulate Processes*. New York: Academic Press.

Renzulli, A. & Santi, P. (1997). Sub-volcanic crystallization at Stromboli (Aeolian Islands, southern Italy) preceding the Sciara del Fuoco sector collapse: Evidence from monzonite lithic suite. *Bulletin of Volcanology* **59**, 10–20.

Resmini, R. G. & Marsh, B. D. (1995). Steady-state volcanism, paleoeffusion rates, and magma system volume from plagioclase crystal size distributions in mafic lavas: Dome Mountain, Nevada. *Journal of Volcanology and Geothermal Research* **68**, 273–296.

Saar, M. O., Manga, M., Cashman, K. V. & Fremouw, S. (2001). Numerical models of the onset of yield strength in crystal–melt suspensions. *Earth and Planetary Science Letters* **187**, 367–379.

Sahagian, D. L. & Proussevitch, A. A. (1998). 3D particle size distributions from 2D observations: Stereology for natural applications. *Journal of Volcanology and Geothermal Research* **84**, 173–196.

Smith, J. V. (1998). Interpretation of domainal groundmass textures in basalt lavas of the southern Lamington Volcanics, eastern Australia. *Journal of Geophysical Research* **103**, 27383–27391.

Spohn, T., Hort, M. & Fischer, H. (1988). Numerical simulation of the crystallization of multicomponent melts in thin dikes or sills: 1—The liquidus phase. *Journal of Geophysical Research* **93**, 4880–4894.

Swanson, S. E. (1977). Relation of nucleation and crystal-growth rate to the development of granitic textures. *American Mineralogist* **62**, 966–978.

Tomiya, A. & Takahashi, E. (1995). Reconstruction of an evolving magma chamber beneath Usu Volcano since the 1663 eruption. *Journal of Petrology* **36**, 617–636.

Toramaru, A. (2001). A numerical experiment of crystallization for a binary eutectic system with application to igneous textures. *Journal of Geophysical Research* **106**, 4037–4060.

Underwood, E. E. (1970). *Quantitative Stereology*. Reading, MA: Addison Wesley.

Zellmer, G. F., Blake, S., Vance, D., Hawkesworth, C. & Turner, S. (1999). Plagioclase residence times at two island arc volcanoes (Kameni Islands, Santorini, and Soufrière, St. Vincent) determined by Sr diffusion systematics. *Contributions to Mineralogy and Petrology* **136**, 345–357.

Zingg, T. (1935). Beitrag zur Schotteranalyse: Die Schotteranalyse und ihre Anwendung auf die Glattalschotter. *Schweizerische Mineralogische und Petrographische Mitteilungen* **15**, 39–140.